Available online at www.sciencedirect.com

ScienceDirect

journal homepage: www.elsevier.com/locate/he

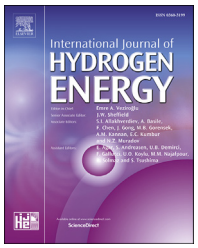

Energy analysis of a class of copper–chlorine (Cu–Cl) thermochemical cycles

Wei Wu [a,*], Han Yu Chen [a], Jenn-Jiang Hwang [b]

[a] Department of Chemical Engineering, National Cheng Kung University, Tainan 70101, Taiwan, ROC
[b] Department of Greenergy, National University of Tainan, Tainan 70005, Taiwan, ROC

ARTICLE INFO

Article history:
Received 8 February 2017
Received in revised form
19 April 2017
Accepted 19 May 2017
Available online 10 June 2017

Keywords:
Hydrogen production
Thermochemical cycle
Copper–chlorine
Energy analysis
Aspen plus

ABSTRACT

For separating water into hydrogen and oxygen through intermediate Cu–Cl compounds, the new system configurations for 5-step, 4-step and 3-step thermochemical cycles using electrolysis of CuCl/HCl or CuCl and Brayton cycle are addressed in Aspen Plus® environment. To address the feasible predictions by thermodynamic systems, we found that (i) the pressure and temperature affect the product yields of CuO * $CuCl_2$ and CuCl in the hydrolysis and oxygen production processes; (ii) the internal heat recovery ratio (IHRR) and the feed ratio of $H_2O/CuCl_2$ dominate the energy efficiencies and Cl_2 production, respectively. Based on the prescribed operating conditions, the comparative evaluations show that the 5-step Cu–Cl cycle using CuCl electrolyzer can ensure the highest energy efficiency while IHRR = 72%, the 3-step Cu–Cl cycle using CuCl electrolyzer can ensure the less equipment and the highest energy efficiency while IHRR = 100%. The 4-step Cu–Cl cycle using CuCl/HCl electrolyzer, where the electrolyzer prevents copper crossovers and safely produces the pure hydrogen gas at low temperature, has a high possibility of commercialization due to the lower grade heat requirement, the less number of equipment and the higher energy efficiency.

Introduction

Hydrogen would become significant in the next several decades since hydrogen has the potential to be used in power generation and transportation. Although the hydrogen production processes using the reforming of natural gas and gasification of coal are commercially available, they would produce massive carbon emissions. To address the hydrogen production process without carbon emissions, the thermochemical water splitting or electrolysis of water are two major technologies. It is well known that electrolysis of water into hydrogen and oxygen requires large amounts of electricity, but thermochemical water splitting can significantly reduce the power consumption if the non-fossil energy sources such as nuclear and solar are available. Currently, the most promising thermochemical water splitting cycles were identified for efficient, cost-effective, large-scale production of hydrogen utilizing high-temperature heat from nuclear power plants [1,2]. The solar-driven thermochemical cycles based on metallic oxides were one of the ultimate options for CO_2-free production of hydrogen, but the selection and evaluation of the promising cycles were performed in the temperature range of 900–2000 °C [3]. The sulfur–iodine (S–I) thermochemical cycle could be suitable to treat exhaust flue gas produced by combustion of sulfur-containing fuels. It has

* *Corresponding author*. Fax: +886 62344496.
E-mail address: weiwu@mail.ncku.edu.tw (W. Wu).
http://dx.doi.org/10.1016/j.ijhydene.2017.05.132

shown that the S–I cycle can result in a significant cost reduction compared to conventional sulfur recovery [4]. Elder and Allen [5] indicated that the cost of hydrogen produced from the S–I cycle by using nuclear technologies is around $2/kg H_2, but the very high temperature reactors are required. To assess the hydrogen production cycle, Yılmaz and Balta [6] showed that the energy and exergy efficiencies of the boron-based thermochemical cycle were 11.00% and 20.34% at 298 K, respectively. Balta et al. [7] showed that the energy and exergy efficiencies of a 4-step copper–chlorine (Cu–Cl) cycle for a geothermal-based hydrogen production process could achieve 21.67% and 19.35%, respectively, under prescribed conditions and parameters. Recently, a novel integrated nuclear plant for electricity and hydrogen production using 4-step Cu–Cl cycle, where hydrogen gas was directly produced by the electrolysis reactor, can achieve about 31.6% energy efficiency [8]. However, the energy demand for Cu–Cl cycle and the hydrogen compression system may consume over 75% of thermal energy output from the nuclear reactor. For a 5-step Cu–Cl thermochemical cycle, its energy efficiency could achieve 44% by virtue of the sensitivity analysis on the basis of the lower heating value of hydrogen [9]. Based on an optimization algorithm for maximizing the thermal efficiency of a 5-step Cu–Cl thermochemical cycle using the heat exchanger network, Sayyaadi and Boroujeni [10] indicated that the thermal efficiency of the cycle was improved by 10.2% compared to previous designs.

The S–I and Cu–Cl thermochemical cycles are promising methods for CO_2-free production of hydrogen, where the Cu–Cl cycle has the advantage of a lower maximum temperature than the S–I cycle [11]. The Cu–Cl cycle can reach the same efficiency as the S–I cycle, while using lower grade heat. The process design for different steps Cu–Cl cycles based on two options of electrolysis of intermediate compounds CuCl and/or HCl, one is hydrogen produced from electrolysis of CuCl/HCl and another is copper produced from electrolysis of CuCl, are investigated with regard to the ratio of recovered energy [12]. They showed that more steps can provide good flexibility, but the less steps induce higher grade heat and intensity requirements. However, the thermal efficiency of Cu–Cl cycles may be strongly affected by using CuCl/HCl and CuCl electrolyzers, respectively. The energy analysis of a 5-step Cu–Cl cycle using electrolysis of CuCl is useful to assist the development of a lab-scale cycle demonstration, e.g. the solid copper conveyor is added to handle copper from the hydrogen production step and the copper production step simultaneously [13]. To reduce the solid material processing and avoid too high temperature hydrogen gas appeared in Cu–Cl cycles, the recent progress on the electrolysis of CuCl/HCl has been reported along with its integration with a concentrated solar radiation system [14]. Regarding the process integration of Cu–Cl system in terms of energy saving and reduction of auxiliary units, a few pathways for CuCl flows between CuCl/HCl electrolysis and hydrolysis process were investigated [15]. Moreover, some research focuses on the studies of CuCl/HCl electrolyzer through experiments and thermodynamic analysis to improve the electrochemical efficiency against copper crossover [16–18]. On the other hand, the possibility of the Cu–Cl commercialization is evaluated for a 3-step Cu–Cl cycle using CuCl electrolysis if the high temperature heat sources from products of oxygen and hydrogen can be completely recovered [19]. However, aqueous $CuCl_2$ from the CuCl electrolyzer is not directly recycled and the cost of feedstock for fresh solid $CuCl_2$ should be taken into account.

Inspired by comparisons of 5-step, 4-step and 3-step Cu–Cl cycles using CuCl/HCl or CuCl electrolyzer [12], we develop the new process designs of six Cu–Cl cycles for generating electricity and products at normal temperature. Based on the regression models for thermophysical properties of compounds in Cu–Cl cycles [20], comparisons of six Cu–Cl cycles with respect to the internal heat recovery ratio (IHRR) are addressed. In Section "A class of Cu–Cl cycles", we introduce the novel design of six Cu–Cl cycles in Aspen Plus environment. In Section "Results and discussion", the possibility of the Cu–Cl commercialization is evaluated according to energy efficiency and operating conditions is investigated.

A class of Cu–Cl cycles

A class of Cu–Cl cycles includes 5-step, 4-step and 3-step thermochemical cycles using electrolysis of CuCl/HCl and CuCl, respectively. Referring to relevant literatures [12,21,22], major reactions with operating conditions in six Cu–Cl cycles are shown in Table 1. Regarding 5-step, 4-step and 3-step Cu–Cl cycles using electrolysis of CuCl/HCl, they are named $Cu–Cl|_5^{H_2}$, $Cu–Cl|_4^{H_2}$ and $Cu–Cl|_3^{H_2}$, respectively. Notably, (i) the hydrolysis reaction of $Cu–Cl|_4^{H_2}$ and $Cu–Cl|_3^{H_2}$ produces the intermediate compound $CuO^* CuCl_2$ in place of $CuO_{(s)}$ and $CuCl_{2(s)}$ in the hydrolysis reaction of $Cu–Cl|_5^{H_2}$; (ii) $CuO^* CuCl_2$ in the oxygen production reaction of $Cu–Cl|_4^{H_2}$ and $Cu–Cl|_3^{H_2}$ can avoid byproduct Cl_2 in $Cu–Cl|_5^{H_2}$. Regarding 5-step, 4-step and 3-step Cu–Cl cycles using electrolysis of CuCl, they are named $Cu–Cl|_5^{Cu}$, $Cu–Cl|_4^{Cu}$ and $Cu–Cl|_3^{Cu}$, respectively. Notably, (i) $CuO^* CuCl_2$ in the hydrolysis reaction of $Cu–Cl|_5^{Cu}$ and $Cu–Cl|_4^{Cu}$ is omitted in $Cu–Cl|_3^{Cu}$; (ii) the operating temperature of hydrogen production reaction in $Cu–Cl|_j^{Cu}$ ($j = 5, 4, 3$) is up to 450 °C which is higher than the hydrogen production in $Cu–Cl|_j^{H_2}$ ($j = 5, 4, 3$) by using the electrolysis of CuCl/HCl at 100 °C.

Process design

To develop the new process design for a class of Cu–Cl cycles using CuCl/HCl and CuCl electrolyzers in Aspen Plus environment, we assume that: (i) the six Cu–Cl cycles carry out complete chemical/electrochemical reactions; (ii) the different separators can perfectly separate different phases of chemicals; (iii) the material recycle is perfect; (iv) the detailed information of piping and instrumentation diagram (P&ID) is not taken into account. Moreover, three process configurations using two types of electrolyzers and a Brayton cycle for generating electricity and products at normal temperature are shown in Figs. 1–3, respectively.

(i) Regarding the system configuration of $Cu–Cl|_5^{H_2}$ in Fig. 1, a mixture of $CuCl_{2(s)}$ and $H_2O_{(l)}$ is heated up to 400 °C by the first heater (H1) and then fed into a spray reactor for hydrolysis of $CuCl_{2(aq)}$ [23] to produce $CuO_{(s)}$,

Table 1 – A class of Cu–Cl cycles.

$Cu-Cl\|_5^{H_2}$		$Cu-Cl\|_4^{H_2}$		$Cu-Cl\|_3^{H_2}$	
#1	$CuCl_{2(aq)} \rightarrow CuCl_{2(s)}$	#1	$CuCl_{2(aq)} \rightarrow CuCl_{2(s)}$	#1	$2CuCl_{2(aq)} + H_2O_{(g)} \rightarrow CuO\ ^{*}\ CuCl_{2(s)} + 2HCl_{(g)}$
Drying	100 °C, 1 atm	Drying	100 °C, 1 atm	Hydrolysis	400 °C, 1 atm
#2	$2CuCl_{2(s)} + H_2O_{(g)} \rightarrow CuO_{(s)} + CuCl_{2(s)} + 2HCl_{(g)}$	#2	$2CuCl_{2(s)} + H_2O_{(g)} \rightarrow CuO\ ^{*}\ CuCl_{2(s)} + 2HCl_{(g)}$		
Hydrolysis	400 °C, 1 atm	Hydrolysis	400 °C, 1 atm		
#3	$CuCl_{2(s)} \rightarrow CuCl_{(l)} + 0.5Cl_{2(g)}$	#3	$CuO\ ^{*}\ CuCl_{2(s)} \rightarrow 2CuCl_{(l)} + 0.5O_{2(g)}$	#2	$CuO\ ^{*}\ CuCl_{2(s)} \rightarrow 2CuCl_{(l)} + 0.5O_{2(g)}$
O_2 production-1	500 °C, 1 atm	O_2 production	500 °C, 1 atm	O_2 production	500 °C, 1 atm
#4	$CuO_{(s)} + 0.5Cl_{2(g)} \rightarrow CuCl_{(l)} + 0.5O_{2(g)}$				
O_2 production-2	500 °C, 1 atm				
#5	$2CuCl_{(l)} + 2HCl_{(l)} \rightarrow 2CuCl_{2(aq)} + H_{2(g)}$	#4	$2CuCl_{(l)} + 2HCl_{(l)} \rightarrow 2CuCl_{2(aq)} + H_{2(g)}$	#3	$2CuCl_{(l)} + 2HCl_{(l)} \rightarrow 2CuCl_{2(aq)} + H_{2(g)}$
Electrolysis	100 °C, 24 bar	Electrolysis	100 °C, 24 bar	Electrolysis	100 °C, 24 bar
$Cu-Cl\|_5^{Cu}$		$Cu-Cl\|_4^{Cu}$		$Cu-Cl\|_3^{Cu}$	
#1	$CuCl_{2(aq)} \rightarrow CuCl_{2(s)}$	#1	$2CuCl_{2(aq)} + H_2O_{(g)} \rightarrow CuO\ ^{*}\ CuCl_{2(s)} + 2HCl_{(g)}$	#1	$2CuCl_{2(aq)} + H_2O_{(g)} \rightarrow 2HCl_{(g)} + 2CuCl_{(l)} + 0.5O_{2(g)}$
Drying	100 °C, 1.01 bar	Hydrolysis	400 °C, 1 atm	O_2 production	500 °C, 1 atm
#2	$2CuCl_{2(s)} + H_2O_{(g)} \rightarrow CuO\ ^{*}\ CuCl_{2(s)} + 2HCl_{(g)}$				
Hydrolysis	400 °C, 1 atm				
#3	$CuO\ ^{*}\ CuCl_{2(s)} \rightarrow 2CuCl_{(l)} + 0.5O_{2(g)}$	#2	$CuO\ ^{*}\ CuCl_{2(s)} \rightarrow 2CuCl_{(l)} + 0.5O_{2(g)}$		
O_2 production	500 °C, 1 atm	O_2 production	500 °C, 1 atm		
#4	$2CuCl_{(l)} \rightarrow CuCl_{2(aq)} + Cu_{(s)}$	#3	$2CuCl_{(l)} \rightarrow CuCl_{2(aq)} + Cu_{(s)}$	#2	$2CuCl_{(l)} \rightarrow CuCl_{2(aq)} + Cu_{(s)}$
Electrolysis	25 °C, 1 atm	Electrolysis	25 °C, 1 atm	Electrolysis	25 °C, 1 atm
#5	$2Cu_{(s)} + 2HCl_{(g)} \rightarrow 2CuCl_{(l)} + H_{2(g)}$	#4	$2Cu_{(s)} + 2HCl_{(g)} \rightarrow 2CuCl_{(l)} + H_{2(g)}$	#3	$2Cu_{(s)} + 2HCl_{(g)} \rightarrow 2CuCl_{(l)} + H_{2(g)}$
H_2 production	450 °C, 24 bar	H_2 production	450 °C, 24 bar	H_2 production	450 °C, 24 bar

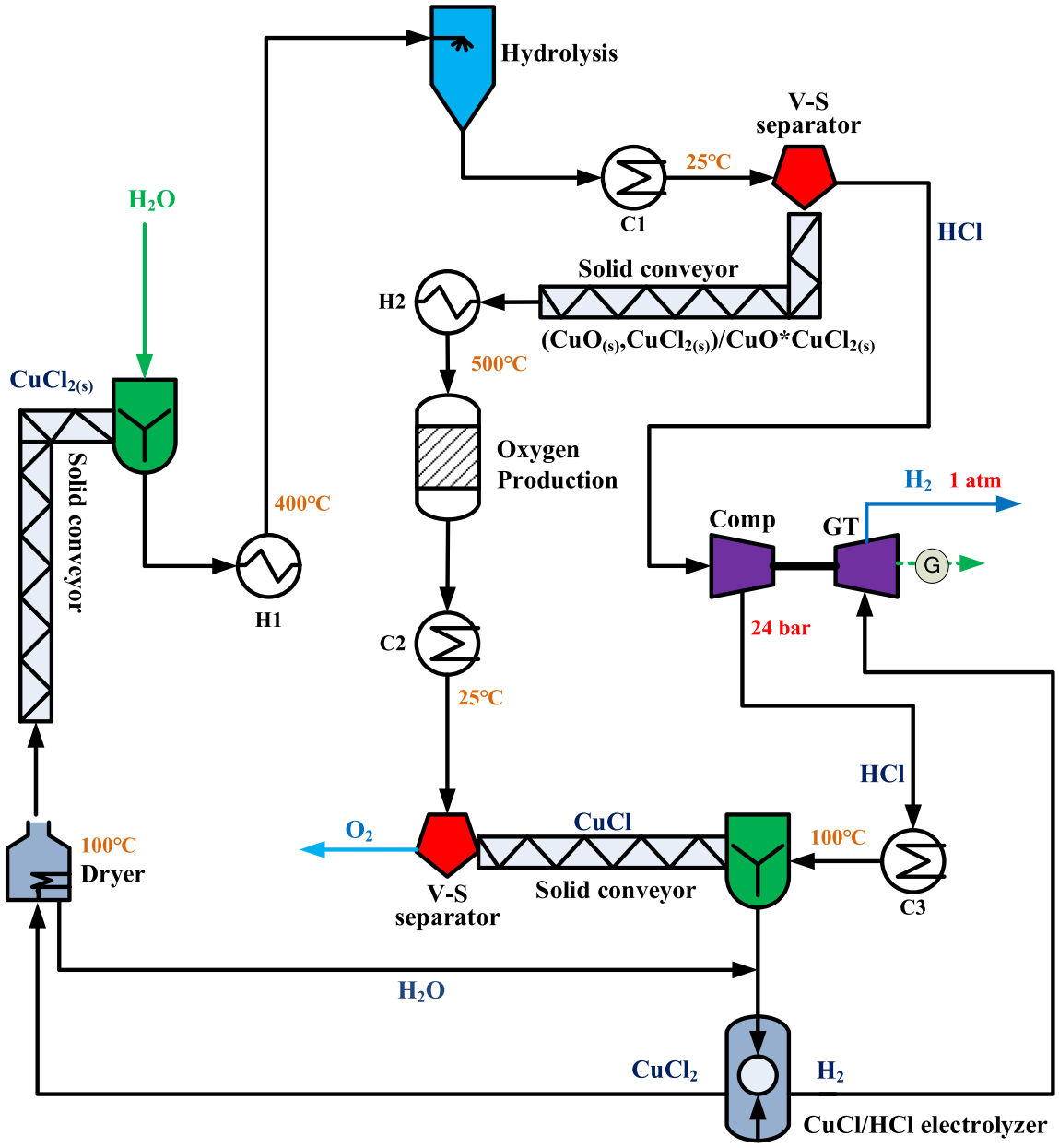

Fig. 1 – Flow chart of Cu–Cl$|_5^{H_2}$ or Cu–Cl$|_4^{H_2}$.

$CuCl_{2(s)}$ and $HCl_{(g)}$. The first cooler (C1) is connected to recover the heat of the outlet stream of the hydrolysis reactor and $HCl_{(g)}$ is obtained by a V-S separator and flows into an isentropic compressor. After the compressor, the temperature of HCl stream is changed from 25 °C to 619 °C, its pressure increases from 1 atm to 24 bar (23.7 atm), and the third cooler (C3) is added to reduce the temperature of the HCl stream from 619 °C to 100 °C. The solid components, $CuO_{(s)}$ and $CuCl_{2(s)}$, are transported through a solid conveyor and then heated by the second heater (H2). Both solid components drop into a vapor–liquid–solid (VLS) reactor to carry out chlorine and oxygen production reactions at 500 °C and 1 atm. Assumed that $CuCl_{2(s)}$, $Cl_{2(g)}$ and $CuO_{(s)}$ can be completely consumed, the outlet stream of the VLS reactor is cooled down to 25 °C by the second cooler (C2) and then $O_{2(g)}$ and $CuCl_{(s)}$ can be completely separated by a V-S separator. The pure O_2 gas is exhausted at 25 °C and 1 atm and $CuCl_{(s)}$ is mixed with HCl at 100 °C. The mixture of $CuCl_{(s)}$, $HCl_{(g)}$ and $H_2O_{(g)}$ flows into a CuCl/HCl electrolyzer to produce $CuCl_{2(aq)}$ at the anode and $H_{2(g)}$ at the cathode if CuCl and HCl can be completely consumed [17]. The aqueous $CuCl_{2(aq)}$ is recycled and becomes the solid $CuCl_{2(s)}$ after the drying process, afterward it is moved by another solid conveyor and mixed with the feedstock. The pure $H_{2(g)}$ stream from the electrolyzer with 100 °C and 24 bar flows into a gas turbine (GT) to produce electricity and it is exhausted at 25 °C and 1 atm. Notably, Cu–Cl$|_5^{H_2}$ becomes Cu–Cl$|_4^{H_2}$ if CuO * $CuCl_2$ is produced in place of

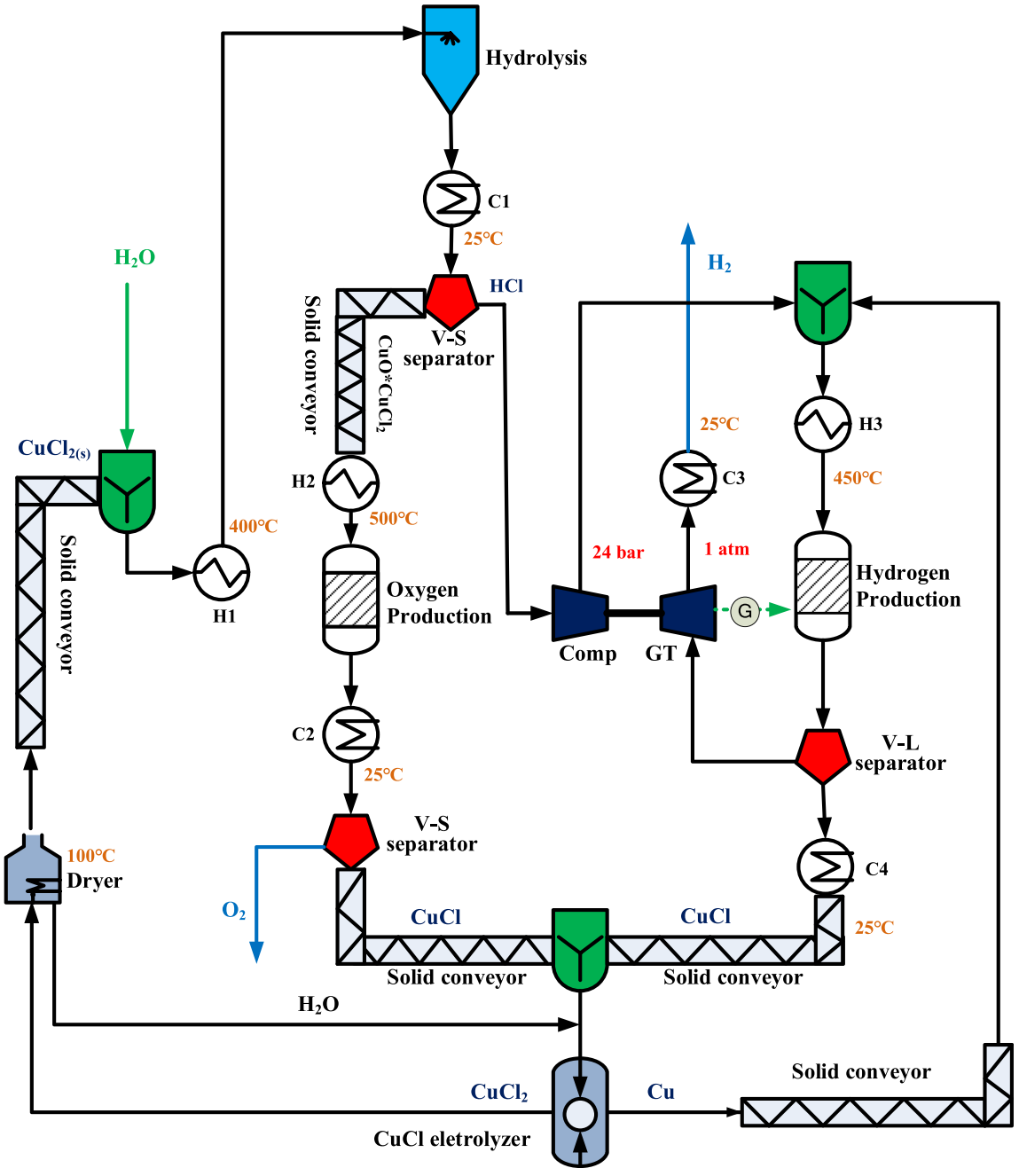

Fig. 2 – Flow chart of Cu–Cl|$^{Cu}_{5}$.

$CuO_{(s)}$ and $CuCl_{2(s)}$ as the intermediate compound in the hydrolysis reaction.

(ii) Regarding the system configuration of Cu–Cl|$^{Cu}_{5}$ in Fig. 2, a mixture of $CuCl_{2(s)}$ and $H_2O_{(l)}$ is heated up to 400 °C by the first heater (H1) and then fed into a spray reactor for hydrolysis of $CuCl_{2(aq)}$ to produce CuO * $CuCl_{2(s)}$ and $HCl_{(g)}$. The first cooler (C1) is connected to the outlet stream of the hydrolysis reactor to reduce the stream temperature from 400 °C to 25 °C, and then $HCl_{(g)}$ and CuO * $CuCl_{2(s)}$ are completely separated by a V-S separator. The HCl gas will flow into an isentropic compressor to increase the pressure from 1 atm to 24 bar. The solid component, CuO * $CuCl_{2(s)}$, is transported through a solid conveyor and then heated by the second heater (H2), afterward, it drops into the first VLS reactor to carry out the oxygen production reaction at 500 °C and 1 atm. Assumed that CuO * $CuCl_{2(s)}$ can be completely consumed, the outlet stream of the first VLS reactor is cooled down to 25 °C by the second cooler (C2) and $O_{2(g)}$ and $CuCl_{(s)}$ is completely separated by a V-S separator. Both $CuCl_{(s)}$ streams through two solid conveyors are mixed with $H_2O_{(g)}$ and flow into a CuCl electrolyzer to produce $CuCl_{2(aq)}$ at the anode and $Cu_{(s)}$ at the cathode at 25 °C and 1 atm if $CuCl_{(aq)}$ can be completely consumed. $Cu_{(s)}$ is recycled by the copper conveyor and mixed with $HCl_{(g)}$ and then heated up to 450 °C by the third heater (H3). The mixture

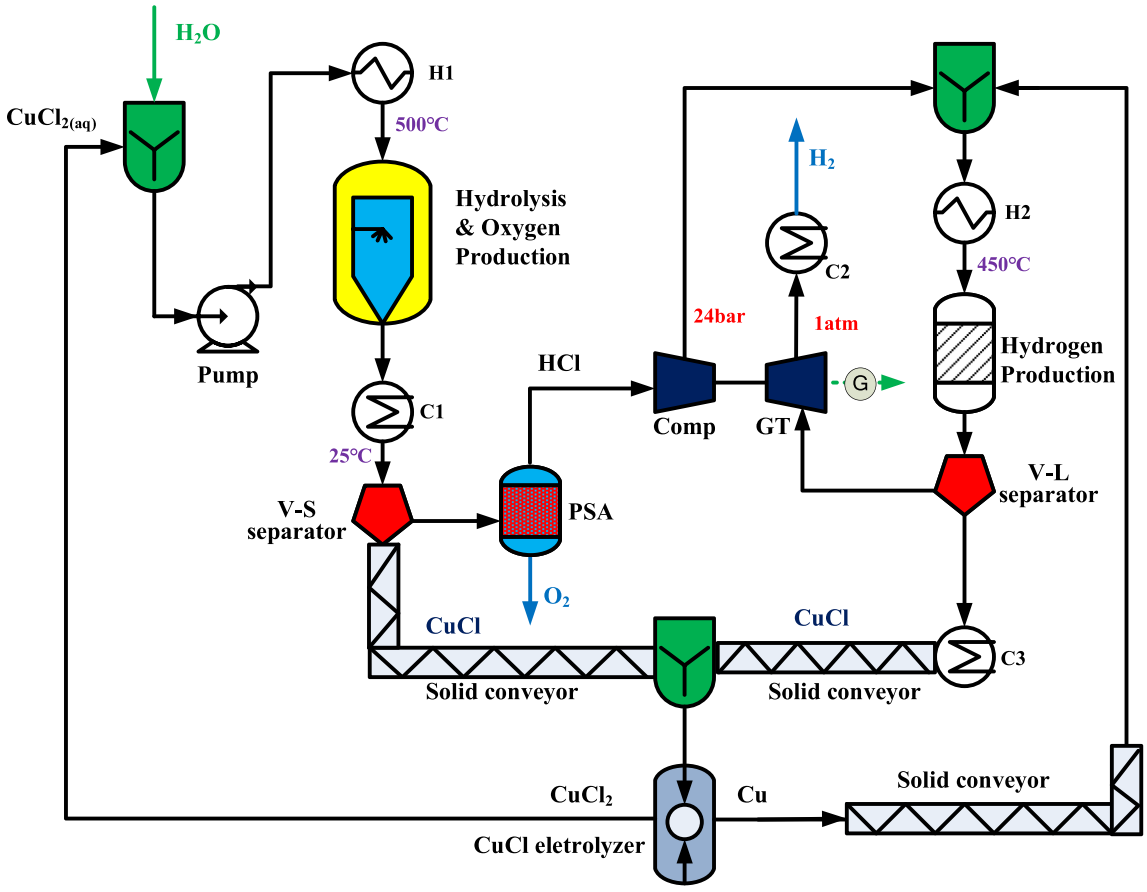

Fig. 3 – Flow chart of $Cu-Cl|_3^{Cu}$.

of $Cu_{(s)}$ and $HCl_{(g)}$ flows into the second VLS reactor to carry out the hydrogen production reaction at 450 °C and 24 bar. The outlet compounds, $H_{2(g)}$ and $CuCl_{(l)}$, are completely separated by a V-L separator. One of the streams by $H_{2(g)}$ directly flows into a gas turbine (GT) to produce electricity and exit at 25 °C after the third cooler (C3), and another stream by $CuCl_{(l)}$ is cooled down by the fourth cooler (C4). The aqueous $CuCl_{2(aq)}$ is recycled and becomes the solid $CuCl_{2(s)}$ after the drying process, then it is moved by a solid conveyor and mixed with the feedstock.

For a comparison of $Cu-Cl|_5^{H_2}$ and $Cu-Cl|_5^{Cu}$, (i) the number of VLS reactors, separators and conveyors in $Cu-Cl|_5^{H_2}$ is less than in $Cu-Cl|_5^{Cu}$, and (ii) $Cu-Cl|_5^{H_2}$ can directly produce the high-purity hydrogen at low temperature but $Cu-Cl|_5^{Cu}$ requires an additional V-L separator to purify hydrogen. Intuitively, the capital cost of $Cu-Cl|_5^{H_2}$ is lower than $Cu-Cl|_5^{Cu}$ if the energy efficiency, corrosions, and undesired side products are not taken into account. Moreover, $Cu-Cl|_4^{H_2}$ becomes $Cu-Cl|_3^{H_2}$ and $Cu-Cl|_5^{Cu}$ becomes $Cu-Cl|_4^{Cu}$ if the drying process is removed and the feedstock is changed to $CuCl_{2(aq)}$ and $H_2O_{(l)}$. To address the compact combination for $Cu-Cl|_3^{Cu}$, the new system configuration is stated as follows.

(iii) In Fig. 3, a mixture of $CuCl_{2(aq)}$ and $H_2O_{(l)}$ flows into a pump to increase pressure from 1 atm to 24 bar (23.7 atm) and then is heated up to 500 °C by the first heater (H1) before it is fed into a fixed-bed reactor for hydrolysis & oxygen production reactions where the formation of CuO * $CuCl_{2(s)}$ is omitted. The outlet stream of this reactor is cooled down to 25 °C by the first cooler (C1) and then connect to a V-S separator to separate the gas-phase compounds of $O_{2(g)}$ and $HCl_{(g)}$ and the solid-phase $CuCl_{(s)}$. The gas-phase stream is connected to a pressure swing adsorption (PSA) to exit the pure $O_{2(g)}$ and recover $HCl_{(g)}$ which flows into an isentropic compressor and then mixed with a recycled $Cu_{(s)}$ at 25 °C. The mixture of $HCl_{(g)}$ and $Cu_{(s)}$ is heated up to 450 °C by the second heater (H2) and flows into a VLS reactor for hydrogen production. The solid-phase $CuCl_{(s)}$ from different reactors are transported by two solid conveyors and flow into a CuCl electrolyzer to produce $CuCl_{2(aq)}$ at the anode and $Cu_{(s)}$ at the cathode at 25 °C and 1 atm if $CuCl_{(s)}$ can be completely consumed. If the complete reaction is achieved, the outlet stream of the reactor contains $H_{2(g)}$ and $CuCl_{(l)}$, where $H_{2(g)}$ directly flows into a gas turbine (GT) to produce electricity and then exits at 25 °C after the second cooler (C2) and $CuCl_{(l)}$ is cooled down by the third cooler (C3). Finally, $CuCl_{2(aq)}$ from a CuCl electrolyzer is directly recycled and mixed with the feedstock.

Notably, a combination of isentropic compressor and gas turbine is denoted as the Brayton cycle [24] which can improve

Table 2 – Energy analysis of Cu–Cl$|_5^{H_2}$.

No.	Major units in cycle route	Operation	Description	H_{in} − IHRR × (H_{out}) (kJ/mol H_2)	Work/electricity (kJ/mol H_2)
1	Drying	25 °C → 100 °C	$CuCl_{2(aq)} \rightarrow CuCl_{2(s)}$	33.62	
2	Heater (H1)	25°C/100 °C → 400 °C	$CuCl_{2(s)}$, $H_2O_{(l)}$	114.15	
3	Hydrolysis	400 °C	$2CuCl_{2(s)} + H_2O_{(g)} \rightarrow CuO_{(s)} + CuCl_{2(s)} + 2HCl_{(g)}$	111.75	
4	Cooler (C1)	400 °C → 25 °C	$HCl_{(g)}$, $CuO_{(s)}$, $CuCl_{2(s)}$	−64.62	
5	Heater (H2)	400 °C → 500 °C	$CuO_{(s)}$, $CuCl_{2(s)}$	54.68	
6	Cl_2 & O_2 production	500 °C	$CuCl_{2(s)} \rightarrow CuCl_{(l)} + 0.5Cl_{2(g)}$ $CuO_{(s)} + 0.5Cl_{2(g)} \rightarrow CuCl_{(l)} + 0.5O_{2(g)}$	98.17	
7	Cooler (C2)	500 °C → 25 °C	$CuCl_{(s)}$, $O_{2(g)}$	−52.55	
8	Compressor	1 atm → 24 bar	$HCl_{(g)}$		34.95
9	Cooler (C3)	619 °C → 100 °C	$HCl_{(g)}$	−30.97	
10	Heater (H3)	30 °C → 100 °C	$CuCl_{(s)}$	6.07	
11	Electrolysis of CuCl/HCl	100 °C	$2CuCl_{(s)} + 2HCl_{(g)} \rightarrow 2CuCl_{2(aq)} + H_{2(g)}$		256.46
12	Gas turbine (GT)	24 bar → 1 atm	$H_{2(g)}$		−4.63
				$\Delta H_{net}^{100\%} = 270.31$	$\Delta P_{net} = 286.77$

Table 3 – Energy analysis of Cu–Cl$|_4^{H_2}$.

No.	Major units in cycle route	Operation	Description	H_{in} − IHRR × (H_{out}) (kJ/mol H_2)	Work/electricity (kJ/mol H_2)
1	Drying	25 °C → 100 °C	$CuCl_{2(aq)} \rightarrow CuCl_{2(s)}$	33.62	
2	Heater (H1)	25°C/100 °C → 400 °C	$CuCl_{2(s)}$, $H_2O_{(l)}$	114.15	
3	Hydrolysis	400 °C	$2CuCl_{2(s)} + H_2O_{(g)} \rightarrow CuO\ ^*\ CuCl_{2(s)} + 2HCl_{(g)}$	109.83	
4	Cooler (C1)	400 °C → 25 °C	$HCl_{(g)}$, $CuO\ ^*\ CuCl_{2(s)}$	−69.30	
5	Heater (H2)	400 °C → 500 °C	$CuO\ ^*\ CuCl_{2(s)}$	60.63	
6	Oxygen production	500 °C	$CuO^*CuCl_{2(s)} \rightarrow 2CuCl_{(l)} + 0.5O_{2(g)}$	98.81	
7	Cooler (C2)	500 °C → 25 °C	$CuCl_{(s)}$, $O_{2(g)}$	−52.55	
8	Compressor	1 atm → 24 bar	$HCl_{(g)}$		34.95
9	Cooler (C3)	619 °C → 100 °C	$HCl_{(g)}$	−30.97	
10	Heater (H3)	30 °C → 100 °C	$CuCl_{(s)}$	6.07	
11	Electrolysis of CuCl/HCl	100 °C	$2CuCl_{(s)} + 2HCl_{(g)} \rightarrow 2CuCl_{2(aq)} + H_{2(g)}$		256.46
12	Gas turbine (GT)	24 bar → 1 atm	$H_{2(g)}$		−4.63
				$\Delta H_{net}^{100\%} = 270.31$	$\Delta P_{net} = 286.77$

the energy efficiency and also compensate the electricity demand of electrolyzer. The number of units in Cu–Cl$|_3^{Cu}$ including reactors, conveyors, separators, and coolers is less than other Cu–Cl cycles but the corresponding operating temperature of the fixed-bed reactor for hydrolysis & oxygen production reactions is up to 500 °C.

Results and discussion

According to the proposed system configurations for six Cu–Cl cycles, the energy evaluations of major devices in each Cu–Cl cycle are shown in Tables 2–7, where thermodynamics models

Table 4 – Energy analysis of Cu–Cl$|_3^{H_2}$.

No.	Major units in cycle route	Operation	Description	H_{in} − IHRR × (H_{out}) (kJ/mol H_2)	Work/electricity (kJ/mol H_2)
1	Heater (H1)	25°C/100 °C → 400 °C	$CuCl_{2(aq)}$, $H_2O_{(l)}$	102.46	
2	Hydrolysis	400 °C	$2CuCl_{2(s)} + H_2O_{(g)} \rightarrow CuO\ ^*\ CuCl_{2(s)} + 2HCl_{(g)}$	442.19	
3	Cooler (C1)	400 °C → 25 °C	$HCl_{(g)}$, $CuO\ ^*\ CuCl_{2(s)}$	−401.66	
4	Heater (H2)	400 °C → 500 °C	$CuO\ ^*\ CuCl_{2(s)}$	60.63	
5	Oxygen production	500 °C	$CuO\ ^*\ CuCl_{2(s)} \rightarrow 2CuCl_{(l)} + 0.5O_{2(g)}$	545.07	
6	Cooler (C2)	500 °C → 25 °C	$CuCl_{(s)}$, $O_{2(g)}$	−498.80	
7	Compressor	1 atm → 24 bar	$HCl_{(g)}$		34.95
8	Cooler (C3)	619 °C → 100 °C	$HCl_{(g)}$	−30.97	
9	Heater (H3)	30 °C → 100 °C	$CuCl_{(s)}$	6.07	
10	Electrolysis of CuCl/HCl	100 °C	$2CuCl_{(s)} + 2HCl_{(g)} \rightarrow 2CuCl_{2(aq)} + H_{2(g)}$		256.46
11	Gas turbine (GT)	24 bar → 1 atm	$H_{2(g)}$		−4.63
				$\Delta H_{net}^{100\%} = 224.99$	$\Delta P_{net} = 286.77$

Table 5 – Energy analysis of Cu–Cl$_5^{Cu}$.

No.	Major units in cycle route	Operation	Description	H_{in} − IHRR × (H_{out}) (kJ/mol H_2)	Work/electricity (kJ/mol H_2)
1	Drying	25 °C → 100 °C	$CuCl_{2(aq)} \rightarrow CuCl_{2(s)}$	37.45	
2	Heater (H1)	25°C/100 °C → 400 °C	$CuCl_{2(s)}$, $H_2O_{(g)}$	128.32	
3	Hydrolysis	400 °C	$2CuCl_{2(s)} + H_2O_{(g)} \rightarrow CuO\ ^{*}\ CuCl_{2(s)} + 2HCl_{(g)}$	135.20	
4	Cooler (C1)	400 °C → 25 °C	$HCl_{(g)}$	−27.10	
5	Heater (H2)	400 °C → 500 °C	$CuO\ ^{*}\ CuCl_{2(s)}$	16.43	
6	Oxygen production	500 °C	$CuO\ ^{*}\ CuCl_{2(s)} \rightarrow 2CuCl_{(l)} + 0.5O_{2(g)}$	121.63	
7	Cooler (C2)	500 °C → 25 °C	$CuCl_{(s)}$, $O_{2(g)}$	−64.68	
8	Electrolysis of CuCl	25 °C	$4CuCl_{(s)} \rightarrow 2CuCl_{2(aq)} + 2Cu_{(s)}$		239.00
9	Compressor	1 atm → 24 bar	$HCl_{(g)}$		34.95
10	Heater (H3)	25 °C → 450 °C	$HCl_{(g)}$, $Cu_{(s)}$	20.61	
11	Hydrogen production	450 °C	$2Cu_{(s)} + 2HCl_{(g)} \rightarrow 2CuCl_{(l)} + H_{2(g)}$	−84.97	
12	Gas turbine (GT)	24 bar → 1 atm	$H_{2(g)}$		−4.63
13	Cooler (C3)	450 °C → 25 °C	$H_{2(g)}$	−3.39	
14	Cooler (C4)	450 °C → 25 °C	$CuCl_{(s)}$	−36.85	
				$\Delta H_{net}^{100\%} = 242.65$	$\Delta P_{net} = 269.32$

Table 6 – Energy analysis of Cu–Cl$_4^{Cu}$.

No.	Major units in cycle route	Operation	Description	H_{in} − IHRR × (H_{out}) (kJ/mol H_2)	Work/electricity (kJ/mol H_2)
1	Pump	1 atm → 24 bar	$CuCl_{2(aq)}$		1.65
2	Heater (H1)	25 °C → 400 °C	$CuCl_{2(aq)}$, $H_2O_{(g)}$	139.59	
3	Hydrolysis	400 °C	$2CuCl_{2(aq)} + H_2O_{(g)} \rightarrow CuO\ ^{*}\ CuCl_{2(s)} + 2HCl_{(g)}$	135.20	
4	Cooler (C1)	400 °C → 25 °C	$HCl_{(g)}$	−27.10	
5	Heater (H2)	400 °C → 500 °C	$CuO\ ^{*}\ CuCl_{2(s)}$	16.43	
6	Oxygen production	500 °C	$CuO\ ^{*}\ CuCl_{2(s)} \rightarrow 2CuCl_{(l)} + 0.5O_{2(g)}$	670.95	
7	Cooler (C2)	500 °C → 25 °C	$CuCl_{(l)}$, $O_{2(g)}$	−614.01	
8	Electrolysis of CuCl	25 °C	$4CuCl_{(l)} \rightarrow 2CuCl_{2(aq)} + 2Cu_{(s)}$		239.00
9	Compressor	1 atm → 24 bar	$HCl_{(g)}$		34.95
10	Heater (H3)	25 °C → 450 °C	$HCl_{(g)}$, $Cu_{(s)}$	20.61	
11	Hydrogen production	450 °C	$2Cu_{(s)} + 2HCl_{(g)} \rightarrow 2CuCl_{(l)} + H_{2(g)}$	−84.97	
12	Gas turbine (GT1)	24 bar → 1 atm	$H_{2(g)}$		−4.63
13	Cooler (C3)	450 °C → 25 °C	$H_{2(g)}$	−3.39	
14	Cooler (C4)	450 °C → 25 °C	$CuCl_{(l)}$	−36.85	
				$\Delta H_{net}^{100\%} = 216.48$	$\Delta P_{net} = 270.96$

of all Cu–Cl components are based on the regression models [20]. In our approach, the energy consumptions of all separators and solid conveyors are not taken into account due to complicated configurations, and auxiliary work is simplified by operating a pump and/or a compressor. To evaluate the possibility of the Cu–Cl commercialization, the sensitivity analysis of specific chemical processes and comparisons of energy efficiencies of Cu–Cl cycles are addressed as follows.

Table 7 – Energy analysis of Cu–Cl$_3^{Cu}$.

No.	Major units in cycle route	Operation	Description	H_{in} − IHRR × (H_{out}) (kJ/mol H_2)	Work/electricity (kJ/mol H_2)
1	Pump	1 atm → 24 bar	$CuCl_{2(aq)}$		1.65
1	Heater (H1)	25 °C → 500 °C	$CuCl_{2(aq)}$, $H_2O_{(g)}$	170.95	
2	Hydrolysis & oxygen production	500 °C	$2CuCl_{2(aq)} + H_2O_{(g)} \rightarrow 2HCl_{(g)} + 2CuCl_{(l)} + 0.5O_{2(g)}$	840.38	
3	Cooler (C1)	500 °C → 25 °C	$HCl_{(g)}$, $CuCl_{(s)}$, $O_{2(g)}$	−716.02	
4	Electrolysis of CuCl	25 °C	$4CuCl_{(s)} \rightarrow 2CuCl_{2(aq)} + 2Cu_{(s)}$		239.00
5	Compressor	1 atm → 24 bar	$HCl_{(g)}$		34.95
6	Heater (H2)	25 °C → 450 °C	$HCl_{(g)}$, $Cu_{(s)}$	19.15	
7	Hydrogen production	450 °C	$2Cu_{(s)} + 2HCl_{(g)} \rightarrow 2CuCl_{(l)} + H_{2(g)}$	−84.97	
8	Gas turbine (GT)	24 bar → 1 atm	$H_{2(g)}$		−4.63
9	Cooler (C2)	450 °C → 25 °C	$H_{2(g)}$	−3.39	
10	Cooler (C3)	450 °C → 25 °C	$CuCl_{(s)}$	−36.85	
				$\Delta H_{net}^{100\%} = 189.25$	$\Delta P_{net} = 270.96$

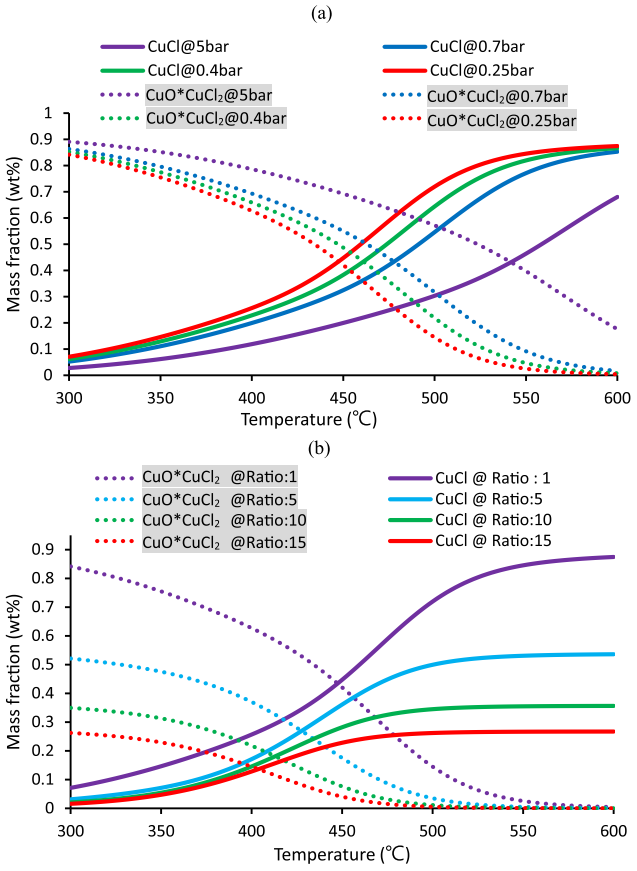

Fig. 4 – Mass fractions of compounds CuO * $CuCl_2$ and CuCl in O_2 production reactor regarding (a) pressure and (b) feed ratio of $H_2O/CuCl_2$.

Sensitivity analysis

To address the large hydrogen production of two types of Cu–Cl cycles using CuCl/HCl electrolyzer and CuCl electrolyzer, first CuCl produced from the oxygen production reaction tends to be high because it dominates both electrolysis reactions, second HCl produced from the hydrolysis reaction tends to be high because it dominates the electrolysis of CuCl/HCl of Cu–$Cl|_i^{H_2}$ and the hydrogen production reaction of Cu–$Cl|_j^{Cu}$. Moreover, the feasible operating conditions are stated as follows.

(i) Using RGibb module of Aspen Plus for Cu–$Cl|_i^{H_2}$ ($i = 4, 3$) and Cu–$Cl|_j^{Cu}$ ($j = 5, 4$) with the same hydrolysis and oxygen production processes, the sensitivity analysis of mass fractions of products, CuO * $CuCl_2$ and CuCl, in the oxygen production process with respect to the effects of pressure and temperature are shown in Fig. 4(a) and (b), respectively. Fig. 4(a) indicates that the mass fraction of CuO * $CuCl_2$ decreases as well as the mass fraction of CuCl increases by increasing the temperature and decreasing the pressure while the feed ratio of H_2O and $CuCl_2$ is fixed at 1. Similarly, Fig. 4(b) indicates that the mass fraction of CuO * $CuCl_2$ decreases as well as the mass fraction of CuCl increases by increasing the temperature as well as increasing the feed ratio of H_2O/$CuCl_2$ while the operating pressure is kept at 1 atm. To keep the higher mass fraction of CuO * $CuCl_2$ in the hydrolysis process, we consider that the temperature is operated at 400 °C and the pressure is kept at 1 atm. To keep the higher mass fraction of CuCl in the oxygen

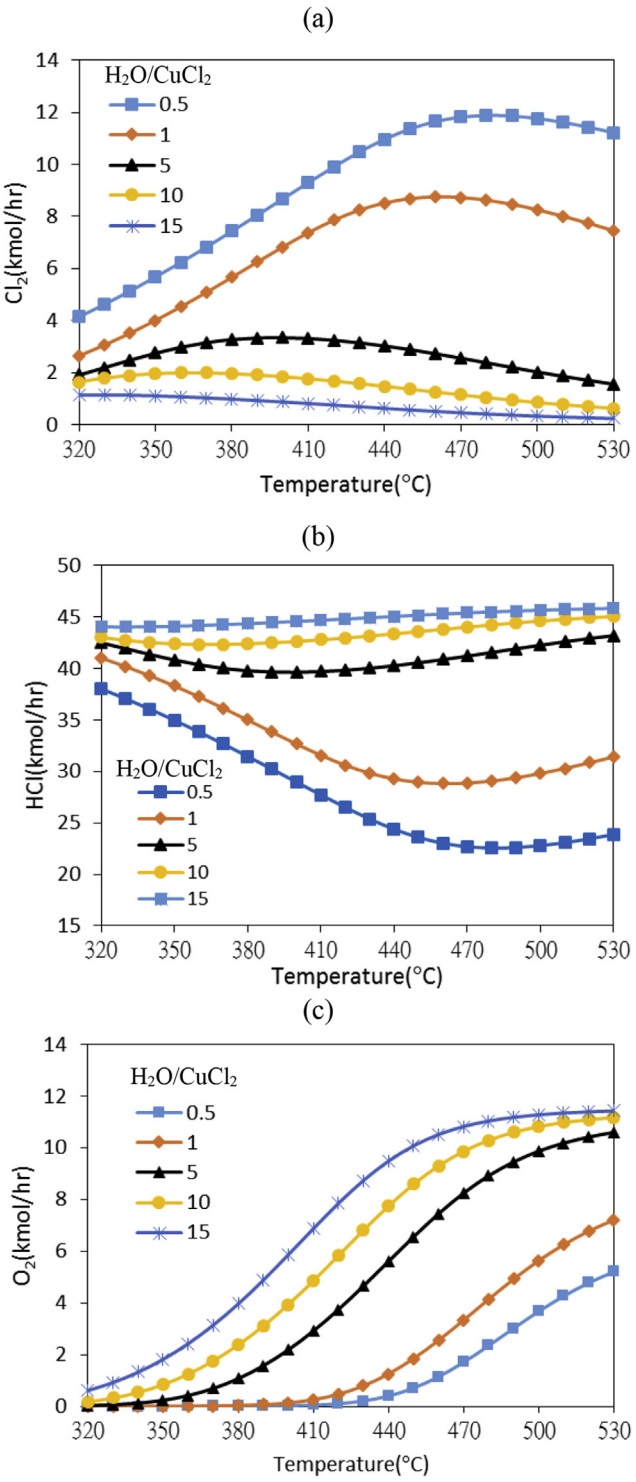

Fig. 5 – Sensitivity analysis of hydrolysis & O_2 production reactor regarding effects of $H_2O/CuCl_2$ and temperature: flow profiles of (a) Cl_2, (b) HCl, and (c) O_2.

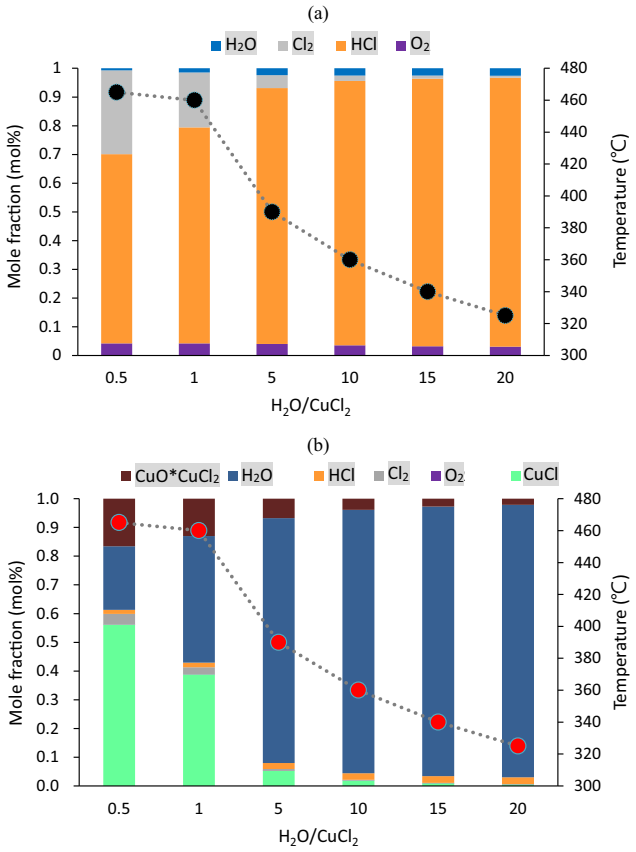

Fig. 6 – Mole fractions of compounds in (a) vapor phase and (b) vaper–liquid–solid phases of hydrolysis & O_2 production reactor regarding effects of $H_2O/CuCl_2$ and temperature.

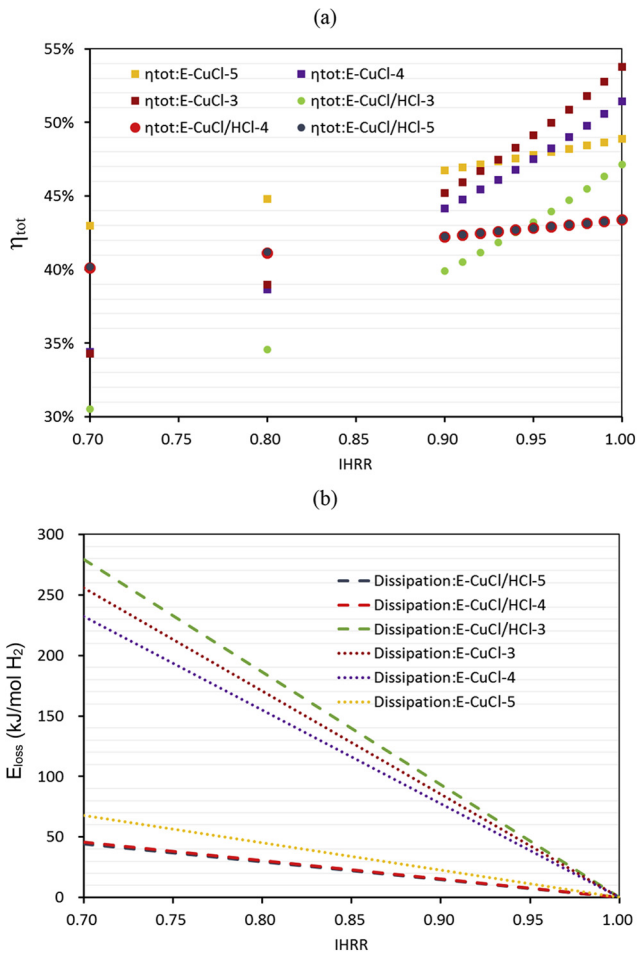

Fig. 7 – Energy evaluations of six Cu–Cl cycles with regard to IHRR: (a) energy efficiency and (b) the corresponding energy dissipation.

production process, we consider that the temperature is operated at 500 °C at least.

(ii) Using RGibb module of Aspen Plus for Cu–$Cl|_5^{H_2}$ and Cu–$Cl|_3^{Cu}$, the Cl_2 production reaction by $CuCl_{2(s)} \rightarrow CuCl_{(l)} + 0.5Cl_{2(g)}$ for producing CuCl and toxic chlorine gas may occur in parallel with its hydrolysis [23,25]. To reduce Cl_2 gas and increase HCl, a reverse Deacon reaction by $Cl_{2(g)} + H_2O_{(g)} \rightarrow 2HCl_{(g)} + 0.5O_{2(g)}$ is expected under desired operating conditions [26]. Referring the experimental design for a hydrolysis and oxygen production process [27], Fig. 5 shows productions of Cl_2, HCl, and O_2 under effects of $H_2O/CuCl_2$ and temperature. By Fig. 5(a), Cl_2 can be almost consumed and diluted by increasing H_2O at the higher temperature. Notably, the increase of H_2O usually increases the energy demand. Fig. 5(b) shows that the excess H_2O, e.g. $H_2O/CuCl_2 = 15$, contributes to increasing HCl at the higher temperature and the corresponding O_2 formation in Fig. 5(c) is also larger. It is noted that the feasible operating conditions are based on $H_2O/CuCl_2 = 15$ and the reactors for oxygen production with operating temperature of 500 °C. Moreover, Fig. 6(a) and (b) shows that Cl_2 gas is dramatically diluted and the mole fractions of $CuO^*CuCl_{2(s)}$ and $CuCl_{(s)}$ are very low, respectively, if the feed ratio of $H_2O/CuCl_2$ achieves 15 and the operating temperature is down below 340 °C.

Energy efficiency

To access the energy performance of proposed system configurations, the energy efficiency calculation for these six cycles is described by

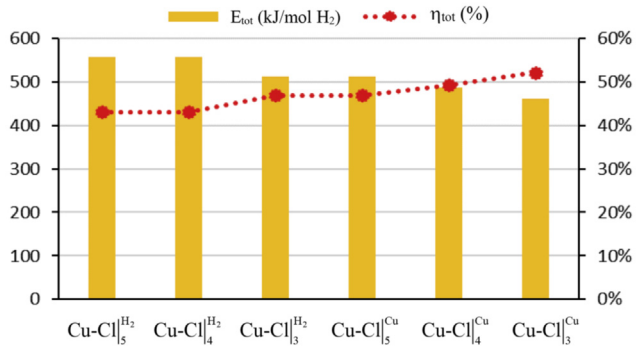

Fig. 8 – Comparisons of six Cu–Cl cycles with IHRR = 100% regarding total energy demand and energy efficiency.

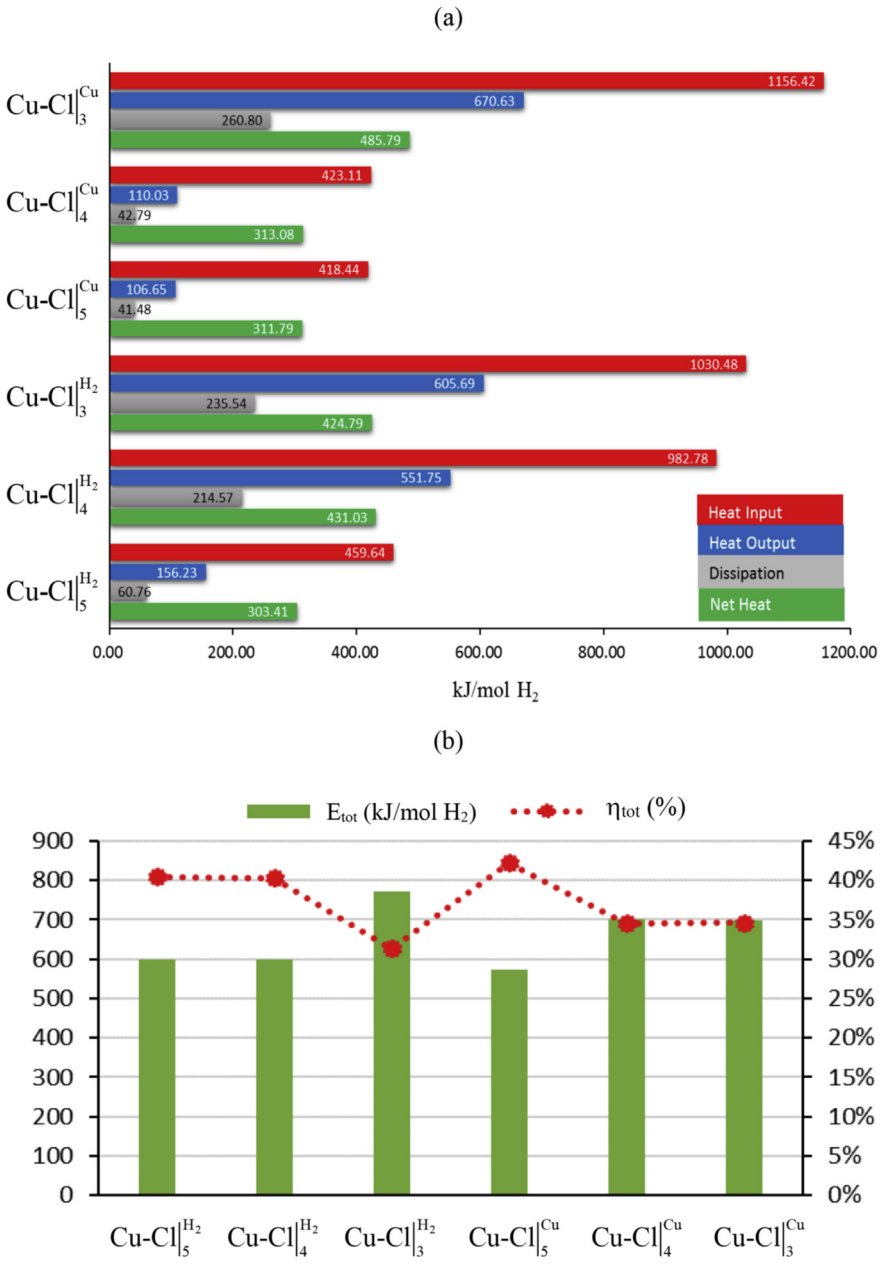

Fig. 9 – Comparisons of a class of Cu–Cl cycles with IHRR = 72%: (a) Enthalpy changes and dissipation, (b) corresponding total energy demand and energy efficiency.

$$\eta_{tot} = \frac{LHV_{H_2}}{\Delta H_{net}^{IHRR} + \Delta P_{net}} \times 100\% \quad (1)$$

where LHV_{H_2} is the lower heating value of hydrogen (240 kJ/mol H_2). ΔP_{net} represents the network including the electricity demand of electrolyzer, pump, compressor and the power generation from the gas turbine. ΔH_{net}^{IHRR} represents the net enthalpy changes regarding reactions, duties of hot/cold utilities.

$$\Delta H_{net}^{IHRR} = \sum H_{in} - IHRR \times \sum H_{out} \quad (2)$$

where H_{in} is the heat input regarding endothermic reactions and heaters, H_{out} is the heat output regarding exothermic reactions and coolers, and a factor $0 \leq IHRR \leq 1$ represents the internal heat recovery ratio. Moreover, IHRR can be used to describe the energy dissipation, E_{loss}, e.g. it can be shown by

$$E_{loss} = (1 - IHRR) \times \sum H_{out} \quad (3)$$

Notably, the process without the energy dissipation implies IHRR = 100%. Actually, the increase of energy dissipation could cover the energy consumptions of IHRR. Based on prescribed operating conditions in Tables 2–7 and $H_2O/CuCl_2 = 15$, the comparisons of six Cu–Cl cycles subject to η_{tot} and E_{loss} are shown in Fig. 7(a) and (b), respectively. We found that Cu–$Cl|_3^{Cu}$ has the highest energy efficiency while IHRR = 100%, Cu–$Cl|_5^{Cu}$ has the highest energy efficiency while IHRR = 72%, and

Cu–Cl$|_3^{H_2}$ has the highest energy dissipation due to the large temperature differences between the inlet and outlet streams of coolers. Notably, these efficiency comparisons are consistent with the previous designs, where the thermal efficiency is an average of 50–60% in thermochemical cycles [12,28]. However, Fig. 7 shows that the energy dissipations and efficiencies of Cu–Cl$|_j^{Cu}$ and Cu–Cl$|_i^{H_2}$ are not only varied by IHRR but also the less step cycles can ensure the higher energy efficiencies if the higher grade heat requirement can be overcome, e.g. IHRR $\geq$ 95%. Furthermore, a few comparisons between Cu–Cl$|_i^{H_2}$ and Cu–Cl$|_j^{Cu}$ are shown as follows.

(i) Fig. 8 shows comparisons of six Cu–Cl cycles with IHRR = 100% regarding the total energy demand and energy efficiency, where the total energy demand, E_{tot}, is the summation of ΔH_{net}^{IHRR} and ΔP_{net}. The energy efficiencies of Cu–Cl$|_j^{Cu}$ (j = 4,3) is higher than Cu–Cl$|_i^{H_2}$ (j = 4, 3) since the total energy demand of Cu–Cl$|_j^{Cu}$ is lower than Cu–Cl$|_i^{H_2}$. Notably, the energy efficiencies of Cu–Cl$|_3^{H_2}$ with η_{tot} = 46.90% and Cu–Cl$|_5^{Cu}$ with η_{tot} = 46.88% are almost the same because the drying process of Cu–Cl$|_3^{H_2}$ is removed.

(ii) Fig. 9(a) shows comparisons of six Cu–Cl cycles regarding $\sum H_{in}$, $\sum H_{out}$ and E_{loss} while IHRR = 72%. Notably, the heat input/output of Cu–Cl$|_3^{H_2}$ are higher than other cycles due to the higher operating temperature of reactors, and E_{loss} and $\Delta H_{net}^{0.72}$ of Cu–Cl$|_5^{H_2}$ are lower than other cycles due to the smaller $\sum H_{out}$.

(iii) Fig. 9(b) shows comparisons of six Cu–Cl cycles with IHRR = 72% regarding the total energy demand and energy efficiency. The energy efficiency of Cu–Cl$|_3^{H_2}$ with η_{tot} = 31.32% is lower than other cycles due to the largest E_{tot} = 772.57 (kJ/mol H_2), and the energy efficiency of Cu–Cl$|_5^{Cu}$ with η_{tot} = 42.25% is higher than other cycles due to the lowest E_{tot} = 572.73 (kJ/mol H_2). It is noted that the energy efficiencies of Cu–Cl$|_4^{H_2}$ and Cu–Cl$|_5^{H_2}$ become higher than Cu–Cl$|_4^{Cu}$ and Cu–Cl$|_3^{Cu}$ while IHRR decreases to 72%.

By Figs. 8 and 9(b), we found that: (i) η_{tot} of Cu–Cl$|_3^{Cu}$ is obviously degraded from 52.77% to 34.86% while IHRR is changed from 100% to 72%; (ii) η_{tot} of Cu–Cl$|_4^{H_2}$ is higher than Cu–Cl$|_4^{Cu}$ or Cu–Cl$|_3^{Cu}$ while IHRR = 72%. To address the compact and high-efficiency system configuration, Cu–Cl$|_3^{Cu}$ with IHRR = 100% is recommended. To evaluate the possibility of the commercialization, Cu–Cl$|_i^{H_2}$ is superior to Cu–Cl$|_j^{Cu}$ since the CuCl/HCl electrolyzer prevents copper crossovers and safely produces the pure hydrogen gas at low temperature, where Cu–Cl$|_4^{H_2}$ is recommended due to the lower grade heat requirement, the less number of equipment and the higher energy efficiency. In addition, Cu–Cl$|_4^{H_2}$ is superior to Cu–Cl$|_5^{H_2}$ because the intermediate compound, CuO * $CuCl_2$, replaces $CuO_{(s)}$ and $CuCl_{2(s)}$ and avoids Cl_2 production reaction.

Conclusions

In this article, we propose the new system configurations of 5-step, 4-step and 3-step thermochemical cycles using electrolysis of CuCl/HCl or CuCl and Brayton cycle for generating electricity and products at normal temperature. The auxiliary equipment of solid conveyor, pump, compressor, gas turbine and hot/cold utilities are used to carry out the solid material processing and increase the ratio of recovered energy. Through thermodynamic calculation, the reducing tendency of Cl_2 and increasing tendency of HCl can be effectively predicted. Based on the feasible operating conditions, e.g. the feed ratio of $H_2O/CuCl_2$ and the reactor temperature, the energy efficiencies of Cu–Cl cycles under prescribed IHRR are consistent with the previous designs. By a few comparisons, we found that the less step Cu–Cl cycles can reduce the number of equipment but their energy dissipations are large. Although the high energy efficiency of Cu–Cl cycles can increase the economic potential, the complicated kinetics and the VLS reactor design would degrade the utilization of power and heat and actually increase the challenge of commercialization.

Acknowledgment

The authors would like to thank the Ministry of Science and Technology of the People's Republic of China for its partial financial support of this research under grant MOST 104-2211-E-006-239.

REFERENCES

[1] Rosen MA. Advances in hydrogen production by thermochemical water decomposition: a review. Energy 2010;35:1068–76.
[2] Yildiz B, Kazimi MS. Efficiency of hydrogen production systems using alternative nuclear energy technologies. Int J Hydrogen Energy 2006;31:77–92.
[3] Abanades S, Charvin P, Flammant G, Nevenu P. Screening of water-splitting thermochemical cycles potentially attractive for hydrogen production by concentrated solar energy. Energy 2006;31:2805–22.
[4] Liberatore R, Lanchi M, Caputo G, Felici C, Giaconia A, Sau S, et al. Hydrogen production by flue gas through sulfur–iodine thermochemical process: economic and energy evaluation. Int J Hydrogen Energy 2012;11:8939–53.
[5] Elder R, Allen R. Nuclear heat for hydrogen production: coupling a very high/high temperature reactor to a hydrogen production plant. Prog Nucl Energy 2009;51:500–25.
[6] Yılmaz F, Balta MT. Energy and exergy analyses of hydrogen production step in boron based thermochemical cycle for hydrogen production. Int J Hydrogen Energy 2017;42:2485–91.
[7] Balta MT, Dincer I, Hepbasli A. Energy and exergy analyses of a new four-step copper–chlorine cycle for geothermal-based hydrogen production. Energy 2010;35:3263–72.
[8] Al-Zareer M, Dincer I, Rosen MA. Development and assessment of a novel integrated nuclear plant for electricity and hydrogen production. Energy Convers Manage 2017;134:221–34.
[9] Orhan MF, Dincer I, Rosen MA. Process simulation and analysis of a five-step copper–chlorine thermochemical water decomposition cycle for sustainable hydrogen production. Int J Energy Res 2014;38:1391–402.
[10] Sayyaadi H, Boroujeni MS. Conceptual design, process integration, and optimization of a solar Cu–Cl

thermochemical hydrogen production plant. Int J Hydrogen Energy 2017;42:2771–89.
[11] Wang ZL, Naterer GF, Gabriel KS, Gravelsins R, Daggupati VN. Comparison of sulfur–iodine and copper–chlorine thermochemical hydrogen production cycles. Int J Hydrogen Energy 2010;35:4820–30.
[12] Orhan MF, Dincer I, Rosen MA. Efficiency comparison of various design schemes for copper–chlorine (Cu–Cl) hydrogen production processes using Aspen Plus software. Energy Convers Manag 2012;63:70–86.
[13] Rosen MA, Naterer GF, Chukwu CC, Sadhankar R, Suppiah S. Nuclear-based hydrogen production with a thermochemical copper–chlorine cycle and supercritical water reactor: equipment scale-up and process simulation. Int J Energy Res 2012;36:456–65.
[14] Naterer GF, Suppiah S, Stolberg, Lewis M, Wang Z, Rosen MA, et al. Process in thermochemical hydrogen production with copper–chlorine cycle. Int J Hydrogen Energy 2015;40:6283–95.
[15] Pope K, Wang Z, Naterer GF. Process integration of material flows of copper chlorides in the thermochemical Cu–Cl cycle. Chem Eng Res Des 2016;109:273–81.
[16] Balashov VN, Schatz RS, Chalkova E, Akinfiev NN, Fedkin MV, Serguei NL. CuCl electrolysis for hydrogen production in the Cu–Cl thermochemical cycle. J Electrochem Soc 2011;158:B266–75.
[17] Soltani R, Dincer I, Tosen MA. Electrochemical analysis of a HCl(aq)/CuCl(aq) electrolyzer: equilibrium thermodynamics. Int J Hydrogen Energy 2016;41:7835–47.
[18] Sathaiyan N, Nandakumar V, Sozhan G, Packiaraj JG, Devakumar ET, Parvatalu D, et al. Hydrogen generation through cuprous chloride–hydrochloric acid electrolysis. Int J Energy Power Eng 2015;4:15–22.
[19] Wu W, Chen HY, Wijayanti F. Economic evaluation of a kinetic-based copper–chlorine (Cu–Cl) thermochemical cycle plant. Int J Hydrogen Energy 2016;41:16604–12.
[20] Zamfirescu C, Dincer I, Naterer GF. Thermophysical properties of copper compounds in copper–chlorine thermochemical water splitting cycles. Int J Hydrogen Energy 2010;35:4839–52.
[21] Orhan MF, Dincer I, Rosen MA. Design of systems for hydrogen production based on the Cu–Cl thermochemical water decomposition cycle: configurations and performance. Int J Hydrogen Energy 2011;36:11309–20.
[22] Naterer GF, Suppiah S, Lewis M, Gabriel K, Dincer I, Rosen MA, et al. Recent Canadian advances in nuclear-based hydrogen production and the thermochemical Cu–Cl cycle. Int J Hydrogen Energy 2009;34:2901–17.
[23] Ferrandon MS, Lewis MA, Alvarez F, Shafirovich E. Hydrolysis of $CuCl_2$ in the Cu–Cl thermochemical cycle for hydrogen production: experimental studies using a spray reactor with an ultrasonic atomizer. Int J Hydrogen Energy 2010;35:1895–904.
[24] https://en.wikipedia.org/wiki/Brayton_cycle.
[25] Ferrandon MS, Lewis MA, Tatterson DF, Gross A, Doizi D, Croizé L, et al. Hydrogen production by the Cu–Cl thermochemical cycle: investigation of the key step of hydrolysing $CuCl_2$ to Cu_2OCl_2 and HCl using a spray reactor. Int J Hydrogen Energy 2010;35:992–1000.
[26] Lewis MA. R&D status for the Cu–Cl thermochemical cycle. Argonne National Laboratory; 2009.
[27] Gabriel KS, Wang Z, Naterer G. Production of hydrogen from water using a thermochemical copper–chlorine cycle. 2014 [US patent: US8628725B2].
[28] Mapamba LS. Simulation of the copper–chlorine thermochemical cycle [M. Eng. dissertation]. North-West University; 2011.